

# Scalar Glueball Mass Reduction at Finite Temperature in SU(3) Anisotropic Lattice QCD

Noriyoshi ISHII

The Institute of Physical and Chemical Research (RIKEN),  
2-1 Hirosawa, Wako, Saitama 351-0198, JAPAN

Hideo SUGANUMA

Tokyo Institute of Technology,  
2-12-1 Ohokayama, Meguro, Tokyo 152-8552, JAPAN

Hideo MATSUFURU

Yukawa Institute for Theoretical Physics, Kyoto University,  
Kitashirakawa-Oiwake, Sakyo, Kyoto 606-8502, JAPAN

We report the first study of the glueball properties at finite temperatures below  $T_c$  using SU(3) anisotropic lattice QCD with  $\beta = 6.25$ , the renormalized anisotropy  $a_s = a_t = 4$  and  $20^3 N_t$  ( $N_t = 35, 36, 37, 38, 40, 43, 45, 50, 72$ ) at the quenched level. From the temporal correlation analysis with the smearing method, about 20% mass reduction is observed for the lowest scalar glueball as  $m_G(T) = 1200 - 100M eV$  for  $0.8T_c < T < T_c$  in comparison with  $m_G \sim 1500 - 1700M eV$  at  $T = 0$ .

PACS numbers: 12.38.Gc, 12.39.Mk, 12.38.Mh, 11.15.Ha

Finite temperature QCD, including the quark gluon plasma (QGP) physics, is one of the most interesting subjects in the quark hadron physics [1, 2, 3]. At high temperature, in accordance with the asymptotic freedom of QCD, the strong interaction among quarks and gluons is expected to be reduced, and there would occur the deconfinement and/or chiral phase transition [1].

For the study of finite temperature QCD, the lattice QCD Monte Carlo simulation provides a reliable method directly based on QCD. For instance, SU(3) lattice QCD simulations at the quenched level show a weak first-order deconfinement phase transition at the critical temperature  $T_c \sim 260M eV$  [4], and full SU(3) QCD simulations show a chiral phase transition at  $T_c = 173(8)M eV$  for  $N_f = 2$  and  $154(8)M eV$  for  $N_f = 3$  in the chiral limit [5]. Above  $T_c$ , most of the nonperturbative properties such as color confinement and spontaneous chiral-symmetry breaking disappear, and quarks and gluons are liberated.

Even below  $T_c$ , there are many model predictions on the change of the hadron properties [2, 6, 7], the mass and the size, due to the change in the inter-quark potential [8, 9] and the partial chiral restoration. As a pre-critical phenomenon of the QCD phase transition, the possible hadron mass shift at the finite temperature or in the finite density is now one of the most interesting subjects in hadron and QGP physics. For instance, the CERES data with the ultra-relativistic heavy-ion collision experiment may indicate the  $\rho$ -meson mass shift [10], and many theoretical studies [11] have been done to explain this experiment.

Nevertheless, lattice QCD studies for thermal properties of hadrons are still inadequate at present because of the difficulty in measuring the hadronic two-point correlators on the lattice at finite temperature. For instance, on the screening-mass measurement [12, 13], this difficulty

is due to the mixture of the large Matsubara frequencies in addition to the absence of technical prescriptions as the smearing method. On the other hand, on the pole-mass measurement, while it is free from the mixture of the Matsubara frequencies, another difficulty arises from the shrink of the physical temporal size  $l = T$  at high temperature. In fact, the pole-mass measurements have to be performed within the limited distance shorter than  $l = (2T)$ , and such a limitation corresponds to  $N_t = 4 - 8$  near  $T_c$  in the ordinary isotropic lattice QCD [4].

To avoid this severe limitation on the temporal size, we adopt an anisotropic lattice where the temporal lattice spacing  $a_t$  is smaller than the spatial one  $a_s$  [8, 14, 15, 16]. We can thus efficiently use a large number of the temporal lattice points as  $N_t \sim 32$  even near  $T_c$ , while the physical temporal size is kept fixed  $l = T = N_t a_t$ . In this way, the number of available temporal data is largely increased, and accurate pole-mass measurements from the temporal correlation become possible [15, 16].

In this paper, we study the glueball at finite temperature from the temporal correlation analysis. We use SU(3) anisotropic lattice QCD at the quenched level, as a necessary first step before attempting to include the effects of dynamical quarks in the future. Even without dynamical quarks, quenched QCD can reproduce well various masses of hadrons, mesons and baryons, and important nonperturbative quantities such as the confining force and the chiral condensate. In quenched QCD, unlike full QCD, the elementary excitations are only glueballs in the confinement phase below  $T_c \sim 260M eV$ . At zero temperature, the lightest physical excitation is a scalar glueball with  $J^{PC} = 0^{++}$  with the mass  $m_G \sim 1500 - 1700M eV$  [16, 17, 18, 19], which is expected to dominate the thermodynamical properties below  $T_c$ .

We consider the glueball correlator [16, 17, 18, 19,

20, 21] in SU(3) lattice QCD<sub>X</sub> as  $G(t) = \text{Tr} \left[ \prod_{\mathbf{x}} O(t; \mathbf{x}) \right]$ ,  $O(t) = \text{Tr} \left[ \prod_{\mathbf{x}} O(t; \mathbf{x}) \right]$ . The summation

over  $\mathbf{x}$  physically means the zero-momentum projection. The glueball operator  $O(t; \mathbf{x})$  is to be properly taken so as to reproduce its quantum number  $J^{PC}$  in the continuum limit. For instance, the simplest composition for the scalar glueball is given as  $O(t; \mathbf{x}) = \text{ReTr} [P_{12}(t; \mathbf{x}) + P_{23}(t; \mathbf{x}) + P_{31}(t; \mathbf{x})] g$ , where  $P_{ij}(t; \mathbf{x})$  is the plaquette operator. With the spectral representation,  $G(t)$  is expressed as  $G(t) = \sum_n c_n e^{-E_n t}$ ,  $c_n = \int d\mathbf{x} \langle \mathcal{O} | \mathcal{O}(t; \mathbf{x}) | \mathcal{O} \rangle$ , where  $E_n$  denotes the energy of the  $n$ -th excited state  $|\mathcal{O}\rangle$ . Here,  $|\mathcal{O}\rangle$  denotes the vacuum, and  $|\mathcal{G}\rangle$  denotes the ground-state glueball. Note that  $c_n$  is a non-negative number with  $c_0 = 1$ . On a fine lattice with the spacing  $a$ , the simple plaquette operator  $P_{ij}(t; \mathbf{x})$  has a small overlap with the glueball ground state  $|\mathcal{G}\rangle$ , and the extracted mass looks heavier owing to the excited-state contamination. This small overlap problem originates from the fact that  $O(t; \mathbf{x})$  has a smaller "size" of  $O(a)$  than the physical peculiar size of the glueball. This problem becomes severer as  $a \rightarrow 0$ . We thus have to improve  $O(t; \mathbf{x})$  so as to have almost the same size as the physical size of the glueball.

One of the systematic ways to achieve this is the smearing method [21, 22, 23]. The smearing method is expressed as the iterative replacement of the original spatial link variables  $U_i(s)$  by the associated fat link variables,  $\bar{U}_i(s)$  in SU(3)<sub>c</sub>, which is defined so as to maximize

$$\text{ReTr} \bar{U}_i^y(s) = \text{Tr} \left[ U_i(s) + \sum_{j \in \mathcal{N}_i} U_j(s) U_i(s) U_j^\dagger(s) \right]; \quad (1)$$

where  $U_i(s) = U^y(s, \hat{i})$ , and  $\mathcal{N}_i$  is a real parameter. Here, the summation is taken only over the spatial direction to avoid the nonlocal temporal extension. Note that  $\bar{U}_i(s)$  holds the same gauge transformation properties with  $U_i(s)$ . We refer to the fat link defined in Eq. (1) as the first fat link  $\bar{U}_i^{(1)}(s)$ . The  $n$ -th fat link  $\bar{U}_i^{(n)}(s)$  is defined iteratively as  $\bar{U}_i^{(n)}(s) = \bar{U}_i^{(n-1)}(s)$  starting from  $\bar{U}_i^{(1)}(s) = \bar{U}_i(s)$  [23]. For the physically extended glueball operator, we use the  $n$ -th smeared operator, the plaquette operator constructed with  $\bar{U}_i^{(n)}(s)$ .

Next, we consider the size of the  $n$ -th smeared operator. Using the linearization and the continuum approximation, we obtain the diffusion equation as [16, 24]

$$\frac{\partial}{\partial n} \langle \mathcal{O} | \bar{U}_i^{(n)}(s) | \mathcal{O} \rangle = D \nabla^2 \langle \mathcal{O} | \bar{U}_i^{(n)}(s) | \mathcal{O} \rangle; \quad (2)$$

where  $a_s$  denotes the spatial lattice spacing.  $\langle \mathcal{O} | \bar{U}_i^{(n)}(s) | \mathcal{O} \rangle$  describes the distribution of the gluon field  $A_i(\mathbf{x}; t)$  in the  $n$ -th smeared plaquette. The  $n$ -th smeared plaquette located at the origin  $\mathbf{x} = \mathbf{0}$  physically means the Gaussian

TABLE I: The lattice QCD result for the lowest scalar glueball mass at finite temperature. The temporal lattice size  $N_t$ , the corresponding temperature  $T$ , the lowest scalar glueball mass  $m_G(T)$ , the maximum ground-state overlap  $C^{\text{max}}$ , uncorrelated  $\chi^2/N_{\text{DF}}$ , the smearing number  $N_{\text{sme}}$ , the number of gauge configurations  $N_{\text{conf}}$  and the glueball size  $R' = \sqrt{\langle \mathcal{O} | \mathcal{O} \rangle^{-2}}$  are listed. The most suitable smearing number  $N_{\text{sme}}$  is determined with the maximum ground-state overlap condition.

$N_t$	$T$ [MeV]	$m_G$ [MeV]	$C^{\text{max}}$	$\chi^2/N_{\text{DF}}$	$N_{\text{sme}}$	$N_{\text{conf}}$	$R'$ [fm]
72	126	1426(29)	0.95(2)	0.018	39	3887	0.54
50	182	1356(28)	0.92(2)	0.016	43	3902	0.57
45	202	1413(27)	0.96(2)	0.043	40	4759	0.55
43	211	1289(71)	0.90(6)	0.030	46	4435	0.59
40	227	1259(46)	0.87(4)	0.015	38	5863	0.53
38	239	1149(53)	0.82(5)	0.000	39	5650	0.54
37	246	1264(28)	0.89(2)	0.012	31	5498	0.48
36	252	1218(47)	0.86(4)	0.004	37	5806	0.52
35	260	1160(44)	0.85(4)	0.010	38	5925	0.53

extended operator with the distribution as [16, 24]

$$P_i(n; \mathbf{x}) = \frac{1}{(4Dn)^{3/2}} \exp \left[ -\frac{\mathbf{x}^2}{4Dn} \right]; \quad (3)$$

Hence the size of the operator is estimated as

$$R' = \sqrt{\frac{6n}{4Dn}} = a_s \sqrt{\frac{6n}{4Dn}}; \quad (4)$$

So far, the smearing method is introduced to carry out the accurate mass measurement by maximizing the ground-state overlap. However, it can be also used to give a rough estimate of the physical glueball size. In fact, once we obtain the maximum overlap with some  $n$  and  $\mathbf{x}$ , the glueball size is estimated with Eq. (4).

We use the SU(3) anisotropic lattice plaquette action

$$S_G = \frac{1}{N_c} \sum_{s; i < j} \text{ReTr} (1 - P_{ij}(s)) + \frac{1}{N_c} \sum_{s; i} \text{ReTr} (1 - P_{i4}(s)) \quad (5)$$

with the plaquette operator  $P_{ij}(s)$  in the  $(i, j)$ -plane. The lattice parameter is fixed as  $2N_c g^2 = 6.25$ , and the bare anisotropy parameter is taken as  $\beta_G = 3.2552$  so as to reproduce the renormalized anisotropy  $a_s = a_t = 4$  [14]. These parameters produce the spatial lattice spacing as  $a_s^{-1} = 2.272(16)$  GeV ( $a_s = 0.087$  fm), and the temporal one as  $a_t^{-1} = 9.088(64)$  GeV ( $a_t = 0.022$  fm). Here, the scale unit is determined by adjusting the string tension as  $\sigma = 427$  MeV from the on-axis data of the static inter-quark potential. The pseudo-heat-bath algorithm is used to update the gauge field configurations on the lattice of the sizes  $2^D N_t$ , with  $N_t = 35; 36; 37; 38; 40; 43; 45; 50; 72$  as listed in Table I. For each temperature, we pick up gauge field configurations every 100 sweeps for measurements, after skipping more than 20,000 sweeps of the thermalization. The

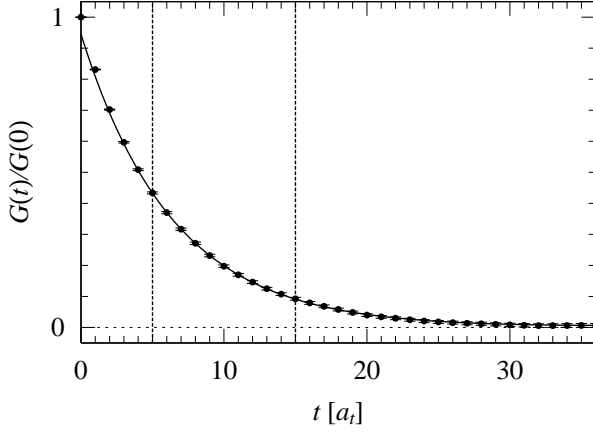


FIG. 1: The scalar glueball correlator  $G(t)=G(0)$  plotted against  $t$  for  $N_{smr} = 40$  at a low temperature  $T = 126\text{ MeV}$ . The statistical errors with the jackknife analysis are hidden within the symbol. The solid curve denotes the best single hyperbolic cosine fit to the lattice data in the interval indicated by the two vertical dashed lines.

numbers of gauge configurations used in our calculations are summarized in Table I.

From the analysis of the Polyakov loop  $\langle P(\mathbf{x}) \rangle = \langle \text{Tr} U_4(\mathbf{x}; 0) \rangle = \langle \text{Tr} U_4(\mathbf{x}; N_t - 1) \rangle$ , we obtain  $T_C \approx 260\text{ MeV}$ , which is consistent with the previous studies [4, 8].

We present the numerical results in SU(3) anisotropic lattice QCD at the quenched level. To enhance the ground-state contribution, we adopt the smearing method with the smearing parameter  $\alpha = 2.1$ , which we find one of the most suitable values from the numerical tests with various  $\alpha$ . The statistical errors are estimated with the jackknife analysis [20].

In Fig. 1, we show a scalar glueball correlator  $G(t)=G(0)$  at a low temperature  $T = 126\text{ MeV}$  for the smearing number  $N_{smr} = 40$ , where most of the lattice QCD data are well fitted by a single hyperbolic cosine, denoted by the solid curve, as

$$G(t)=G(0) = C (e^{-m_G t a_t} + e^{-m_G (N_t - t) a_t}): \quad (6)$$

This indicates the achievement of the ground-state enhancement owing to the smearing method, and then the excited-state contamination is almost removed.

In general,  $G(t)=G(0)$  is expressed as a weighted sum of hyperbolic cosines with non-negative weights, and  $G(t)=G(0)$  decreases more rapidly than Eq. (6) near  $t = 0$  due to excited-state contributions. Hence,  $C$  should satisfy the inequality  $C \leq (1 + e^{-m_G a_t N_t})^{-1} \approx 1$ . In the ground-state dominant case,  $G(t)=G(0)$  can be well approximated by a single hyperbolic cosine, and  $C \approx 1$  is realized. We refer to  $C$  as the ground-state overlap.

From Fig. 1, we find  $C \approx 1$  and  $m_G \approx 1426\text{ MeV}$  for the lowest scalar glueball mass at a low temperature. This seems consistent with  $m_G \approx 1500\text{--}1700\text{ MeV}$  at  $T \approx 0$  [17, 18, 19].

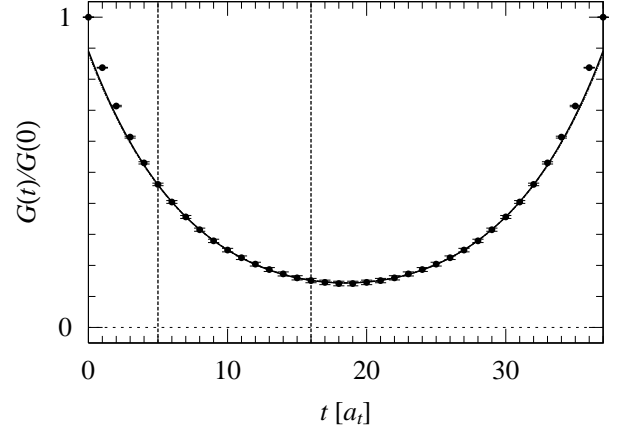


FIG. 2: The scalar glueball correlator  $G(t)=G(0)$  plotted against  $t$  for  $N_{smr} = 40$  at a high temperature  $T = 246\text{ MeV}$ . The statistical errors are hidden within the symbol. The solid curve denotes the best single hyperbolic cosine fit to the lattice data in the interval  $[t_{min}; t_{max}]$  indicated by the two vertical dashed lines. The dashed and dotted curves are the best hyperbolic cosine curves for the modified  $t$  range with  $t_{min} + 1$  and  $t_{min} + 2$ , respectively. The closeness of the three curves means smearing independence.

In Fig. 2, we show a scalar glueball correlator  $G(t)=G(0)$  at a high temperature  $T = 246\text{ MeV}$  for the smearing number  $N_{smr} = 40$ . Owing to a suitable smearing, most of the lattice QCD data are well fitted by a single hyperbolic cosine denoted by the solid curve.

We perform the best fit analysis in the interval  $[t_{min}; t_{max}]$ , which is determined from the flat region  $[t_{min}; t_{max} - 1]$  appeared in the corresponding effective mass plot. The effective mass  $m_e(t)$  is a solution of

$$\frac{G(t+1)}{G(t)} = \frac{\cosh(m_e(t) a_t (t+1 - N_t = 2))}{\cosh(m_e(t) a_t (t - N_t = 2))}; \quad (7)$$

for a given  $G(t+1)=G(t)$  at each fixed  $t$  [20]. In Fig. 2, we show also the results of further two fits in the modified intervals  $[t_{min} + 1; t_{max}]$  and  $[t_{min} + 2; t_{max}]$  by dashed line and dotted line, respectively. The closeness of the three curves suggests smearing independence.

In the most suitable smearing  $N_{smr}$ , the ground-state overlap  $C$  is maximized and the mass  $m_G$  is minimized, which indicates the achievement of the ground-state enhancement. (For extremely large  $N_{smr}$ , the operator size exceeds the physical glueball size, resulting in the decrease of the overlap  $C$ .) In practical calculations, the maximum overlap and the mass minimization are achieved at almost the same  $N_{smr}$ , and both of these two conditions would work as an indication of the maximal ground-state enhancement. Here, we take the maximum ground-state overlap condition as  $C \approx 1$ . (The mass minimization condition leads to almost the same glueball mass [24].)

The main results of this paper are the following two: (I) From the analysis at various temperatures, we plot

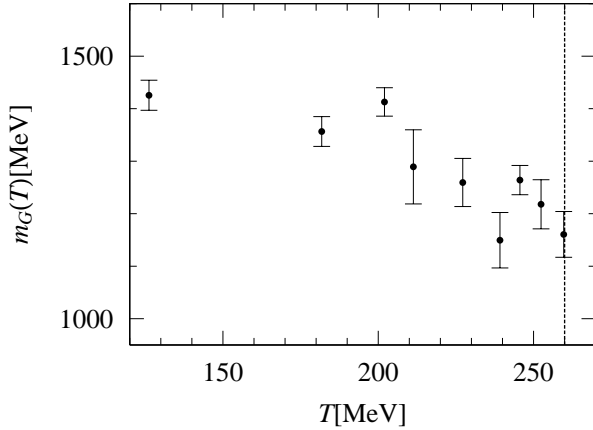


FIG. 3: The lowest scalar glueball mass plotted against the temperature  $T$ . It is obtained with the best hyperbolic cosine fit in the interval  $[t_{min}; t_{max}]$  determined from the flat region in the effective mass plot. The vertical dotted line indicates  $T_c \approx 260$  MeV.

the lattice QCD result for the lowest scalar glueball mass  $m_G(T)$  against temperature  $T$  in Fig. 3. We observe, in Fig. 3, about 20% mass reduction or a few hundred MeV mass reduction of the lowest scalar glueball near  $T_c$  as  $m_G(T) = 1200 - 100$  MeV for  $0.8T_c < T < T_c$  in comparison with  $m_G(T=0) \approx 1500 - 1700$  MeV [17, 18, 19].

(II) To estimate the glueball size, we search  $N_{smr}$  which realizes the maximum ground-state overlap  $C^{max}$ . From Eq. (4) with this  $N_{smr}$ , we estimate the glueball size as  $R \approx 0.5 - 0.6$  fm both at low temperature and at high temperature near  $T_c$ .

In Table I, we summarize the lowest scalar glueball mass  $m_G(T)$ , the ground-state overlap  $C^{max}$ , uncorrelated  $\chi^2/N_{DF}$ , the corresponding smearing number  $N_{smr}$ ,

the number of gauge configurations  $N_{conf}$  and the glueball size  $R$ .

Thus, the present lattice QCD calculation indicates that the lowest scalar glueball exhibits about 250 MeV mass reduction near  $T_c$  keeping its size. Here, we briefly discuss the physical consequence of this result, considering the trigger of the QCD phase transition. In quenched QCD below  $T_c$ , the lowest glueball is the lightest particle, and its thermal excitation is expected to have primary relevance at finite temperature. However, lattice QCD indicates  $m_G > 1$  GeV even near  $T_c$ , and therefore the thermodynamical contribution of the glueball seems strongly suppressed by the small statistical factor as  $e^{-m_G/T}$  near  $T_c \approx 260$  MeV [16, 24]. This may indicate that the thermal glueball excitation does not play the relevant role in the deconfinement phase transition, at least in quenched QCD. Then, what is the driving force to bring the phase transition? In this way, our result brings up such an interesting new puzzle on the QCD phase transition.

To summarize, we have studied the glueball properties at finite temperature using SU(3) anisotropic quenched lattice QCD with more than 3,000 gauge configurations at each temperature. From the temporal correlation analysis with the smearing method, we have observed about 20% mass reduction of the lowest scalar glueball as  $m_G(T) = 1200 - 100$  MeV for  $0.8T_c < T < T_c$ , while no significant change is seen for meson masses near  $T_c$  in lattice QCD [15]. Our result shows that the scalar glueball mass reduction is about 250 MeV, which is enough large. Hence, the thermal mass shift of the scalar glueball may become observable in the future experiment in RHIC.

H. S. is supported by Grant for Scientific Research (No.12640274) from the Ministry of Education, Culture, Science and Technology, Japan. The lattice calculations have been performed on NEC-SX5 at Osaka University.

- 
- [1] W. Greiner and A. Schafer, "Quantum Chromodynamics", (Springer-Verlag, Berlin, 1994) 1.
- [2] T. Hashimoto, K. Hirose, T. Kanki and O. Miyamura, Phys. Rev. Lett. 57, 2123 (1986).
- [3] T. Matsui and H. Satz, Phys. Lett. B 178, 416 (1986).
- [4] G. Boyd, J. Engels, F. Karsch, E. Laermann, C. Legeland, M. Lutgemeier, B. Petersson, Nucl. Phys. B 469, 419 (1996).
- [5] F. Karsch, E. Laermann and A. Peikert, Nucl. Phys. B 605, 579 (2001).
- [6] T. Hatsuda, T. Kunihiro, Phys. Rev. Lett. 55, 158 (1985).
- [7] H. Ichie, H. Suganuma, H. Toki, Phys. Rev. D 52, 2944 (1995).
- [8] H. Matsuura et al., Proc. of Quantum Chromodynamics and Color Confinement, edited by H. Suganuma et al. (World Scientific, 2001) 246.
- [9] O. Kaczmarek, F. Karsch, E. Laermann and M. Lutgemeier, Phys. Rev. D 62, 034021 (2000).
- [10] CERES Collaboration, Phys. Rev. Lett. 75, 1272 (1995).
- [11] V. L. Eletsky, B. L. Io, J. I. Kapusta, Eur. Phys. J. A 3, 381 (1998); Nucl. Phys. A 661, 514 (1999).
- [12] C. DeTar and J. B. Kogut, Phys. Rev. Lett. 59, 399 (1987).
- [13] S. Datta and S. Gupta, Nucl. Phys. B 534, 392 (1998).
- [14] T. R. Klassen, Nucl. Phys. B 533, 557 (1998).
- [15] QCD-TARO Collaboration, Phys. Rev. D 63, 054501 (2001).
- [16] N. Ishii, H. Suganuma and H. Matsuura, Proc. of Lepton Scattering, Hadrons and QCD, edited by A. W. Thom et al. (World Scientific, 2001) 252.
- [17] C. J. Morningstar and M. Peardon, Phys. Rev. D 60, 034509 (1999), and references therein.
- [18] J. Sexton, A. Vaccarino and D. Weingarten, Phys. Rev. Lett. 75, 4563 (1995), and references therein.
- [19] M. J. Teper, OUP-98-88-P (1998), hep-th/9812187.
- [20] I. Montvay and G. Münster, Quantum Fields on a Lattice, (Cambridge, 1994) 1.
- [21] H. J. Rothe, Lattice Gauge Theories, (World Scientific, 1992) 1.
- [22] APE Collaboration, Phys. Lett. B 192, 163 (1987).
- [23] T. T. Takahashi, H. Matsuura, Y. Nemoto and H. Suganuma, Phys. Rev. Lett. 86, 18 (2001).

[24] N. Ishii, H. Suganuma and H. Matsufuru, in preparation.